

# Towards Low-Energy Electron High-Resolution Spectroscopy with Transition-Edge Sensors

R. Ammendola,<sup>1</sup> A. Apponi,<sup>2</sup> G. Benato,<sup>3,4</sup> M.G. Betti,<sup>5,6</sup> R. Biondi,<sup>3,4</sup> P. Bos,<sup>7,8</sup> M. Cadeddu,<sup>9</sup> A. Casale,<sup>10</sup> O. Castellano,<sup>2,11</sup> G. Cavoto,<sup>5,6</sup> L. Cecchini,<sup>5</sup> E. Celasco,<sup>12,13</sup> M. Chirico,<sup>5,6</sup> W. Chung,<sup>14</sup> A.G. Cocco,<sup>3</sup> A.P. Colijn,<sup>7,8</sup> B. Corcione,<sup>5,6,\*</sup> N. D'Ambrosio,<sup>3</sup> M. D'Incecco,<sup>3</sup> G. De Bellis,<sup>5,15</sup> M. De Deo,<sup>3</sup> N. de Groot,<sup>16</sup> A. Esposito,<sup>5,6</sup> M. Farino,<sup>14</sup> S. Farion,<sup>12</sup> A.D. Ferella,<sup>3,17</sup> L. Ferro,<sup>9,18</sup> L. Ficcadenti,<sup>5</sup> G. Galbato Muscio,<sup>5,19</sup> S. Gariazzo,<sup>20,21,22</sup> H. Garrone,<sup>20,23,24</sup> F. Gatti,<sup>12,13</sup> F. Malnati,<sup>20,23,25</sup> G. Mangano,<sup>26,27</sup> L.E. Marcucci,<sup>28,29</sup> C. Mariani,<sup>5,6</sup> J. Mead,<sup>7,8</sup> G. Menichetti,<sup>29</sup> M. Messina,<sup>3</sup> E. Monticone,<sup>20,23</sup> M. Naafs,<sup>7</sup> S. Nagorny,<sup>3,4</sup> V. Narcisi,<sup>1,30</sup> F. Pandolfi,<sup>5</sup> R. Pavarani,<sup>9,18</sup> C. Pepe,<sup>23,31</sup> C. Pérez de los Heros,<sup>32</sup> O. Pisanti,<sup>26,27</sup> F.M. Pofi,<sup>3,4</sup> A.D. Polosa,<sup>5,6</sup> I. Rago,<sup>5</sup> M. Rajteri,<sup>20,23</sup> S. Ritarossi,<sup>2,11</sup> N. Rossi,<sup>3</sup> A. Ruocco,<sup>2,11</sup> G. Salina,<sup>1</sup> A. Santucci,<sup>9,18</sup> M. Sestu,<sup>9,18</sup> A. Tan,<sup>14</sup> V. Tozzini,<sup>28,33</sup> C.G. Tully,<sup>14</sup> I. van Rens,<sup>16</sup> F. Virzi,<sup>3,17</sup> G. Visser,<sup>7</sup> and M. Viviani<sup>28</sup>

<sup>1</sup>*INFN Sezione di Roma Tor Vergata, Roma, Italy*

<sup>2</sup>*INFN Sezione di Roma Tre, Roma, Italy*

<sup>3</sup>*INFN Laboratori Nazionali del Gran Sasso (LNGS), L'Aquila, Italy*

<sup>4</sup>*Gran Sasso Science Institute (GSSI), L'Aquila, Italy*

<sup>5</sup>*INFN Sezione di Roma, Roma, Italy*

<sup>6</sup>*Dipart. di Fisica, Sapienza Università di Roma, Roma, Italy*

<sup>7</sup>*Nationaal instituut voor subatomaire fysica (NIKHEF), Amsterdam, The Netherlands*

<sup>8</sup>*Dept. of Physics, University of Amsterdam, Amsterdam, The Netherlands*

<sup>9</sup>*INFN Sezione di Cagliari, Cagliari, Italy*

<sup>10</sup>*Dept. of Physics, Columbia University, New York, USA*

<sup>11</sup>*Dipart. di Scienze, Università degli Studi di Roma Tre, Roma, Italy*

<sup>12</sup>*INFN Sezione di Genova, Genova, Italy*

<sup>13</sup>*Dipart. di Fisica, Università di Genova, Genova, Italy*

<sup>14</sup>*Princeton University, Princeton NJ, USA*

<sup>15</sup>*Dipart. di Ingegneria Elettrica ed Energetica (DIEE), Sapienza Università di Roma, Roma, Italy*

<sup>16</sup>*Dept. of Physics, Radboud University, Nijmegen, The Netherlands*

<sup>17</sup>*Dipart. di Fisica, Università degli Studi dell'Aquila, L'Aquila, Italy*

<sup>18</sup>*Dipart. di Fisica, Università di Cagliari, Cagliari, Italy*

<sup>19</sup>*Dipart. di Ingegneria Astronautica, Elettrica ed Energetica, Sapienza Università di Roma, Roma, Italy*

<sup>20</sup>*INFN Sezione di Torino, Torino, Italy*

<sup>21</sup>*Dipart. di Fisica, Università di Torino, Torino, Italy*

<sup>22</sup>*Instituto de Fisica Corpuscular (IFIC - CSIC/UV), Paterna (Valencia), Spain*

<sup>23</sup>*Istituto Nazionale di Ricerca Metrologica (INRiM), Torino, Italy*

<sup>24</sup>*Dipart. di Elettronica & Telecomunicazioni (POLITO-ELN), Politecnico di Torino, Torino, Italy*

<sup>25</sup>*Dipart. Scienza Applicata e Tecnologia, Politecnico di Torino, Torino, Italy*

<sup>26</sup>*INFN Sezione di Napoli, Napoli, Italy*

<sup>27</sup>*Dipart. di Fisica, Università degli Studi di Napoli Federico II, Napoli, Italy*

<sup>28</sup>*INFN Sezione di Pisa, Pisa, Italy*

<sup>29</sup>*Dipart. di Fisica, Università di Pisa, Pisa, Italy*

<sup>30</sup>*Dept. of Fusion and Technology for Nuclear Safety and Security, ENEA, Frascati, Italy*

<sup>31</sup>*Instituto de Microelectrónica de Barcelona (IMB-CNM-CSIC), Barcelona, Spain*

<sup>32</sup>*Dept. of Physics and Astronomy, Uppsala University, Uppsala, Sweden*

<sup>33</sup>*CNR-Instituto Nanoscienze, Pisa, Italy*

We present a study of the energy resolution of transition-edge sensors (TESs) for the detection of electrons in the 100 eV kinetic energy range. The TES is a Ti-Au bilayer with an active area of  $(60 \times 60) \mu\text{m}^2$  and a critical temperature of  $\sim 80$  mK. The electron source is based on vertically-aligned multiwall carbon nanotubes located inside the cryostat, with electrons generated via field emission. For electrons in the (92 – 99) eV kinetic energy range, we obtain a Gaussian energy resolution for fully-absorbed electrons of  $(0.479 \pm 0.041 \pm 0.055)$  eV. When considering the full-width at half-maximum of the peak, the corresponding resolution is of  $(1.44 \pm 0.17 \pm 0.27)$  eV. The former represents an improvement of (46 – 60)% with respect to previous results, and is mainly attributed to the reduction in the TES active area. The latter is instead an improvement of over a factor of 20, and is mainly due to the reduction in the emitting area of the electron source, which significantly suppresses electron back-scattering in proximity of the TES. These results represent a major milestone toward high-precision spectroscopy on low-energy electrons, which is a key objective for the PTOLEMY experiment.

\* Corresponding author. E-mail: benedetta.corcione@uniroma1.it

## I. INTRODUCTION

Transition-Edge Sensors (TESs) are microcalorimeters with intrinsic energy resolution capable of detecting single particles over a wide energy spectrum [1–7]. They consist of a superconductive thin film operated at the steep superconductive transition near its critical temperature  $T_C$ , where the resistance of the material is most sensitive to temperature changes [8]. When a particle hits the TES, its energy is deposited into the device via excitations of the lattice and the electronic system, leading to an increase in the TES temperature. This heating produces measurable changes in the TES resistance, which are proportional to the absorbed energy. Such detection mechanism provides the TES with an intrinsic energy resolution, making it particularly suitable to detect small energy transfers. TES devices have been extensively used as high-precision low-energy single-photon detectors, on which they have reached a Gaussian energy resolution below 50 meV for 0.8 eV photons [9, 10].

Recently TES devices have been tested for electron detection, as they offer unique possibilities compared to other devices such as micro-channel plates or silicon-based detectors. In fact TES devices, in principle, have no dead layers and a unitary fill factor [11–13], enabling full collection and measurement of the energy deposited in the device. Moreover, the dark count rates of such devices is  $\mathcal{O}(\text{mHz})$  [14], making them suitable to search for rare events. These characteristics are crucial to make TES devices excellent detectors with intrinsic energy resolution, which is why this technology could play a pivotal role in low-energy electron spectroscopy [15], microcalorimetry [16, 17] and experiments studying  $\beta$ -decay and neutrino physics. Among the latter, the PTOLEMY project [18–20] plans to detect the cosmic neutrino background and measure the mass of the neutrino by analyzing the endpoint of the  $\beta^-$  decay spectrum of atomic tritium. To reach these objectives, PTOLEMY requires a Gaussian energy resolution of 50 meV on electrons with a kinetic energy of 10 eV. To date, a Gaussian energy resolution  $\sigma_e > 17$  eV has been achieved on electrons in the 300 – 2000 eV energy range [15], and  $0.7 < \sigma_e < 1.6$  eV on electrons with kinetic energy  $91 \leq E_e \leq 101$  eV [21, 22]. These latter results appear promising for the PTOLEMY application, so modifications to the experimental setup were implemented to investigate them further.

This work presents new results in which a TES device is used to measure the energy of electrons with kinetic energy in the  $\sim 100$  eV range. Compared to the results presented in the previous work of [21], where a TES with an active area of  $(100 \times 100) \mu\text{m}^2$  and an electron source based on field emission from a  $9 \text{ mm}^2$  carbon nanotube sample were employed, this work uses a  $(60 \times 60) \mu\text{m}^2$  TES and a  $1 \text{ mm}^2$  carbon nanotube source. As shown be-

low, the smaller TES improves the intrinsic energy resolution for fully absorbed electrons, while the reduced source size decreases electron backscattering in the proximity of the TES, thereby greatly suppressing signals from electrons with sub-nominal energy. Together, these changes reduce the width of the electron energy peak by more than an order of magnitude.

## II. EXPERIMENTAL SETUP

The measurements presented in this work are performed at the Innovative Cryogenic Laboratory of the Istituto Nazionale di Ricerca Metrologica (INRiM) in Torino (Italy). An adiabatic demagnetization refrigerator cryostat is used to maintain the TES at a stable bath temperature. Since magnetic fields affect the trajectories of electrons and the read-out system based on dc-SQUIDS [23], a magnetic shield is mounted within the cryostat to surround the whole working area.

The TES used for this work is a bilayer made of 15 nm of titanium and 30 nm of gold, with an active area of  $(60 \times 60) \mu\text{m}^2$  and a critical temperature  $T_C$  of  $\sim 80$  mK. More details on its fabrication are reported in [21]. Its dark count rate is found to be negligible relative to the signal rate at the selected trigger threshold, which is consistent with what is expected from this kind of devices [14].

A sample of vertically-aligned multiwall carbon nanotubes (CNTs) is used as an electron source, as they have proven to be a reliable field-emitter at cryogenic temperatures [24]. They were synthesized in the INFN laboratory ‘TITAN’ at Sapienza University of Rome [24–28] by chemical vapor deposition on a  $500 \mu\text{m}$  silicon substrate, following the procedure described in [24], and covering an area of  $\sim 1 \text{ mm}^2$ .

The CNTs are positioned in front of the TES and are voltage-biased with a negative voltage  $V_{\text{CNT}}$  to emit electrons through field emission, while the TES is electrically grounded through the cryostat and thermally connected to it. As explained in more detail in [21], to adapt the design of the TES for electron detection, a gold shield is deposited everywhere on the substrate except on the active area of the device, in order to protect both the wiring and the insulating substrate from impinging electrons, as the active area of the TES is much smaller than that of the CNTs.

According to Fowler-Nordheim theory [29], the field-emitted current increases exponentially with the applied voltage. A large electron current hitting the gold shield layer has two adverse effects: first it causes an excessive increase in the TES temperature, which in turn decreases the TES dynamic range; secondly, some electrons are back-scattered from the gold shield

layer and then enter the TES with only a fraction of their nominal energy, thus broadening their otherwise monochromatic energy spectrum. Both these aspects can be mitigated by decreasing the area of the CNT source, as fewer electrons are sent towards the device.

The kinetic energy of field-emitted electrons when they reach the TES is derived in [21] as:

$$E_e = eV_{\text{CNT}} - \phi_{\text{TES}} \quad (1)$$

where  $e$  is the elementary electric charge and  $\phi_{\text{TES}}$  is the TES work function. The latter was measured with ultra-violet photoemission spectroscopy in the LASEC lab of Roma Tre University [24], yielding a value of  $\phi_{\text{tes}} = (4.38 \pm 0.03)$  eV. Moreover, CNTs can be considered a monochromatic source, as the energy spread of the field-emitted electrons is negligible at the temperature and electric field ranges of the experiment [30].

The TES is polarized at 35% of its normal resistance, where it was found to be optimal in terms of energy resolution. To ensure stable working conditions, the TES is operated in electrothermal feedback, with the bath temperature approximately set at half the critical temperature of the device. The read-out consists of a dc-SQUID array [23] coupled through a 6 nH inductance. To guarantee a more stable voltage supply and to improve the signal-to-noise ratio on the SQUID readout, a low-pass filter with cutoff frequency of 200 Hz is introduced on the power line of the CNTs at the 3 K stage of the cryostat. Moreover, to reduce the high-frequency noise on the pulse shapes, the signals are pre-processed with a Moku:Lab FPGA-based unit by Liquid Instruments, using a Bessel 100 kHz low-pass filter. Since no such filter was used in the work presented in [21], we have re-processed those data by introducing an additional software-based RC low-pass filter with a cutoff frequency of 100 kHz, so as to allow for a more rigorous comparison.

### III. DATA ANALYSIS

The red histogram in Figure 1 shows the TES signal amplitude spectrum for electrons with a kinetic energy of 96 eV, and is compared to the same spectrum obtained in [21], which is shown in black in the inset. In both the distributions, the peak in the high-amplitude region is associated to events in which the electrons deposit all their energy inside the device, so it was called “full-absorption peak”. As can be seen, the tail to the left of the full-absorption peak is significantly less pronounced in the data of this work. This is mainly due to the smaller CNT sample size, which leads to fewer electrons back-scattering off the gold shield and hitting the TES active area with lower-than-nominal energy.

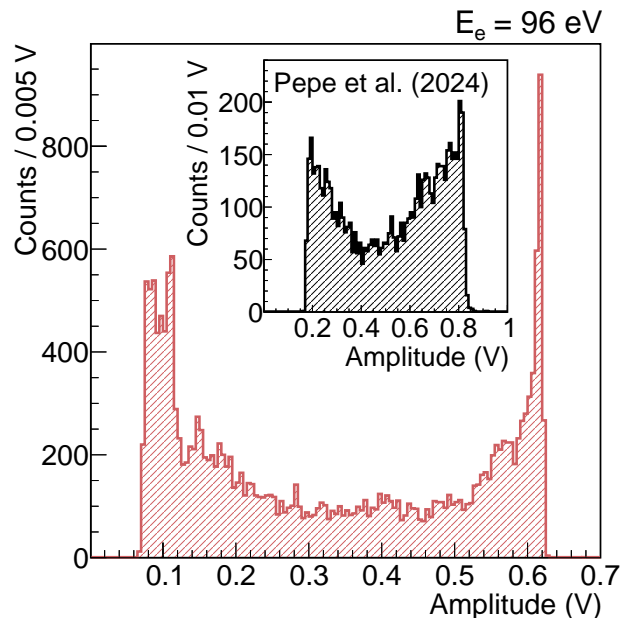


FIG. 1. Signal amplitude spectrum for 96-eV electrons (red histogram), compared to the same spectrum obtained in the previous measurement [21](black histogram in the inset).

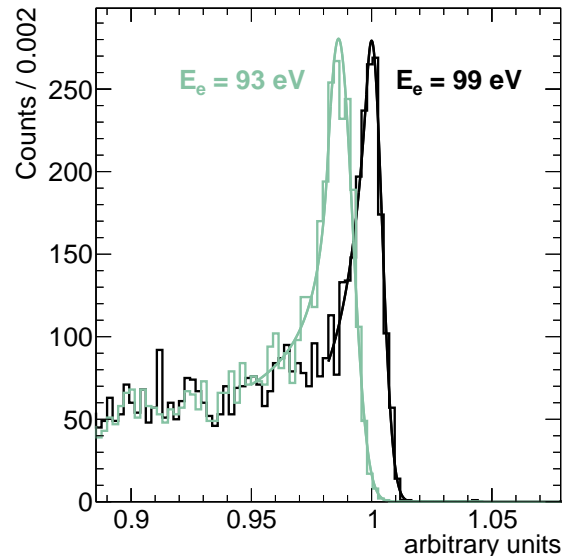


FIG. 2. Example fits of the electron absorption peaks: the green data corresponds to electrons with a kinetic energy  $E_e = 93$  eV, the black data to  $E_e = 99$  eV.

The absorption peaks of the distributions are fitted with a Crystal Ball function [31]: its right side with respect to the peak position ( $\mu$ ) is Gaussian with standard deviation  $\sigma$ ; its left side is Gaussian up to a transition point, where it becomes a power-law tail. In particular,  $\sigma$  is dominated by the energy resolution of the device, whereas the power-law tail describes partially-absorbed electrons. Figure 2 shows two typical fits to the absorp-

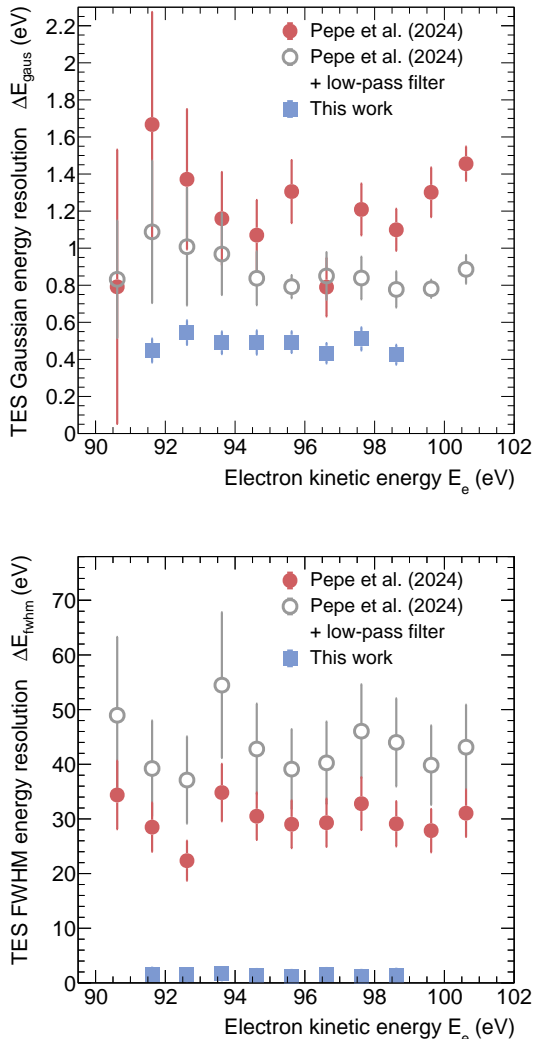


FIG. 3. Top: TES Gaussian energy resolution  $\Delta E_{\text{gaus}}$  for electrons, as a function of their kinetic energy  $E_e$ . Bottom: TES full-width at half-maximum resolution  $\Delta E_{\text{fwhm}}$  for electrons, as a function of their kinetic energy  $E_e$ .

tion peaks: the data corresponding to electrons with a kinetic energy of 93 (99) eV is shown in green (black). As for the data presented in [21] and post-filtered, they are fitted with an asymmetric Gaussian function, as explained in the previous work.

The electron energy resolution is defined using both  $\sigma_R$  and the full-width at half-maximum FWHM, respectively as  $\Delta E_{\text{gaus}} = (\sigma/\mu) \cdot E_e$  and  $\Delta E_{\text{fwhm}} = (\text{FWHM}/\mu) \cdot E_e$ , where the electron kinetic energy  $E_e$  is defined in Equation 1. Figure 3 shows the energy resolutions  $\Delta E_{\text{gaus}}$  and  $\Delta E_{\text{fwhm}}$  achieved by this work (blue squares). These are in turn compared to the data recorded in [21], both in their original form (full red circles) and after the application of a 100 kHz low-pass filter (open gray circles). These results are also summarized in Table I.

As discussed in the Experimental Setup section, the

data reported in [21] were re-processed using a low-pass filter matched to the signal conditioning employed in the present work, in order to enable a consistent comparison. Under these conditions, the re-processed dataset exhibits an improvement of approximately 26% in  $\Delta E_{\text{gaus}}$  with respect to the raw data. Using the present setup, we obtain a Gaussian energy resolution of  $\langle \Delta E_{\text{gaus}} \rangle = (0.479 \pm 0.041 \pm 0.055)$  eV, where the average has been made across the full energy range, and the first uncertainty is statistical and the second is systematic. This corresponds to a 60% (46%) improvement over the raw (filtered) data of our previous work. The improvement with respect to the filtered data is roughly in line with the expected  $\sim 40\%$  improvement in TES energy resolution coming from the reduction in the TES active area. In fact, the intrinsic energy resolution of a TES device is known to be proportional to the square root of its active area [8]. These results indicate that the observed performance enhancement in the present work is primarily driven by detector design rather than by differences in signal filtering.

The FWHM of the absorption peak, on the other hand, is strongly influenced by the reduced size of the CNT emitting area. As shown in Figure 3, we obtain, when averaging across the full electron energy range,  $\langle \Delta E_{\text{fwhm}} \rangle = (1.44 \pm 0.17 \pm 0.27)$  eV. This corresponds to an improvement of a factor 21 (30) with respect the raw (filtered) data of our previous work. It is worth noting that, differently from the case of  $\Delta E_{\text{gaus}}$ , in this case the resolution of our previous setup is worsened by the application of the low-pass filter. In fact, while the width of the right tail of the absorption peak is mainly driven by electronic noise and therefore benefits from filtering, its left tail, in the case of [21], is largely dominated by unwanted signals that persist even after filtering.

The main systematic uncertainty concerns the choice of the model. To estimate this, the systematic uncertainty of the  $\Delta E_{\text{gaus}}$  is calculated by evaluating the variation in energy resolution obtained by using an asymmetric Gaussian instead of a Crystal Ball. This results in a value of 12% for the data of this work, determined as the difference in  $\Delta E_{\text{gaus}}$  obtained with the two different functions, averaged across all tested voltages. To estimate the systematic uncertainty on  $\Delta E_{\text{fwhm}}$ , the FWHM calculated from the fit is compared to the FWHM derived directly from the distribution of the data. The resulting systematic uncertainties are 19%, 14% and 18% for the new data, the previous data, and the previous data post-filtered, respectively, all averaged on the voltages studied. The total uncertainty reported in the error bars of Figure 3 represents the quadrature sum of the statistical contribution and the systematic contribution. The  $\Delta E_{\text{gaus}}$  of the data already presented in [21] (full red circles) is shown as originally published, and to allow for a more rigorous comparison, no additional uncertainty is added to the

Dataset	TES area ( $\mu\text{m}^2$ )	CNT area ( $\text{mm}^2$ )	$E_e$ (eV)	$\langle\Delta E_{\text{gaus}}\rangle$ (eV)	$\langle\Delta E_{\text{fwhm}}\rangle$ (eV)
Pepe et al. 2024 (raw)	$100 \times 100$	9	91 – 101	$1.20 \pm 0.26$	$30.0 \pm 3.5$
Pepe et al. 2024 (low-pass filter)	$100 \times 100$	9	91 – 101	$0.89 \pm 0.10$	$43.2 \pm 5.1$
This work	$60 \times 60$	1	92 – 99	$0.479 \pm 0.041$	$1.44 \pm 0.17$

TABLE I. Summary of TES energy resolution results. The values reported in the last two columns correspond, respectively, to the average  $\Delta E_{\text{gaus}}$  and  $\Delta E_{\text{fwhm}}$  values obtained on the studied electron energy range. Uncertainties are statistical in nature.

corresponding filtered dataset (open gray circles), to which the same uncertainties reported in [21] are applied.

In addition to improving the TES energy resolution, reducing the emitting surface of the electron source mitigates the heating effect associated with field-emission observed in [21]. This aspect is illustrated in Figure 4, where the values of Joule power  $P_J$  required to bring the TES to its working point on the superconductive transition are plotted with respect to the applied bias voltage  $V_{\text{CNT}}$ . In order to compare different measurements, each dataset is normalized to the Joule power dissipated at the lowest  $V_{\text{CNT}}$  analyzed. As can be seen, in the data of this work (blue squares) no relevant heating is present, as the Joule power needed to polarize the TES at its operating temperature remains stable. In the previous data (red circular markers), instead, an exponential reduction of the Joule power  $P_J$  dissipated through the TES with increasing  $V_{\text{CNT}}$  can be observed, indicating a corresponding increase of the substrate temperature. Operating the TES under consistent conditions ensures that measurements performed at different  $V_{\text{CNT}}$  values, corresponding to different electron kinetic energies, can be rigorously compared without applying additional corrections. We have furthermore verified that the peak position  $\mu$  of the Crystal Ball fit function increases linearly with  $V_{\text{CNT}}$ , confirming the stability of the TES working conditions.

#### IV. CONCLUSIONS

We have presented an updated measurement of the TES energy resolution when detecting electrons in the 100-eV kinetic energy range. Compared to our previous work [21], we have employed a TES with a smaller active area of  $(60 \times 60) \mu\text{m}^2$ , and a smaller electron source, based on field emission from a  $(1 \times 1) \text{mm}^2$  chip of vertically-aligned carbon nanotubes (CNTs). We report a remarkable improvement in the energy resolution, both in the Gaussian width of the full-absorption peak ( $\Delta E_{\text{gaus}}$ ), and in the full-width at half-maximum broadness of the peak ( $\Delta E_{\text{fwhm}}$ ). When averaging the results over the full energy range, we obtain  $\langle\Delta E_{\text{gaus}}\rangle = (0.479 \pm 0.041 \pm 0.055) \text{ eV}$ , which corresponds to a 60% improvement with respect to the raw data of our previous work, and to a 46%

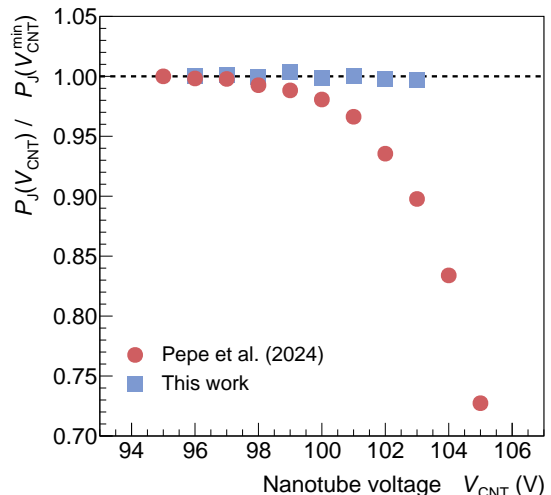


FIG. 4. Joule power  $P_J$  needed to bring the TES to its working point for different values of  $V_{\text{CNT}}$ , normalized to the Joule power needed for the lowest  $V_{\text{CNT}}$  value. A black dashed line corresponding to unity is plotted to guide the eye.

improvement with respect to that same data after the application of a low-pass filter with a frequency of 100 kHz. This improvement is in line with the expectations deriving from the reduction of the TES active area. Taking the same average on  $\Delta E_{\text{fwhm}}$  yields  $\langle\Delta E_{\text{fwhm}}\rangle = (1.44 \pm 0.17 \pm 0.27) \text{ eV}$ , which corresponds to an improvement of a factor 21 (30) with respect to the raw (filtered) data of our previous work. This large improvement, of over an order of magnitude, is mainly due to the reduction in the CNT source size, and represents a major step forward in the spectroscopy of low-energy electrons.

To keep testing the potential of TES devices with electrons, lower energies will be tested by inserting a decelerating plate inside the experimental setup. This will allow us to reach the energy range  $E_e \sim 10 \text{ eV}$  required by the PTOLEMY collaboration.

## V. ACKNOWLEDGEMENTS

The authors are grateful to Elio Bertacco, Martina Marzano, Matteo Fretto and Ivan De Carlo for technical support. This research was partially funded by the contribution of grant 62313 from the John Templeton Foundation, by PRIN grant ‘ANDROMEaDa’

(PRIN 2020Y2JMP5) and PRIN grant ‘TES4e’ (PRIN 2022 202285H5MT) of Ministero dell’Università e della Ricerca, and from the EC project ATTRACT (Grant Agreement No. 777222). We also acknowledge funding from the Agencia Estatal de Investigación (Ref. CNS2023-145234).

- 
- [1] J. Gildemeister, A. T. Lee, and P. Richards, *Applied Physics Letters* **74**, 868 (1999).
- [2] K. Irwin, *Applied Physics Letters* **66**, 1998 (1995).
- [3] B. Cabrera, R. Clarke, P. Colling, A. Miller, S. Nam, and R. Romani, *Applied Physics Letters* **73**, 735 (1998).
- [4] D. T. Chow, A. Loshak, M. L. van den Berg, M. A. Frank, T. W. Barbee Jr, and S. E. Labov, in *Hard X-Ray, Gamma-Ray, and Neutron Detector Physics II*, Vol. 4141 (SPIE, 2000) pp. 67–75.
- [5] G. Angloher, P. Bauer, N. Ferreira, D. Hauff, A. Tanzke, R. Strauss, M. Kiefer, F. Petricia, F. Reindl, W. Seidel, *et al.*, *Journal of Low Temperature Physics* **184**, 323 (2016).
- [6] T. Saab, R. Clarke, B. Cabrera, R. Abusaidi, and R. Gaitskell, *Nuclear Instruments and Methods in Physics Research Section A: Accelerators, Spectrometers, Detectors and Associated Equipment* **444**, 300 (2000).
- [7] A. Orlando, V. Ceriale, G. Ceruti, M. De Gerone, M. Faverezani, E. Ferri, G. Gallucci, A. Giachero, A. Nucciotti, A. Puiiu, *et al.*, *Journal of Low Temperature Physics* **193**, 771 (2018).
- [8] K. D. Irwin and G. C. Hilton, in *Cryogenic particle detection* (Springer, 2005) pp. 63–150.
- [9] L. Lolli, E. Taralli, C. Portesi, E. Monticone, and M. Rajter, *Applied Physics Letters* **103**, 041107 (2013).
- [10] K. Hattori, T. Konno, Y. Miura, S. Takasu, and D. Fukuda, *Superconductor Science and Technology* **35**, 095002 (2022).
- [11] A. Apponi, F. Pandolfi, I. Rago, G. Cavoto, C. Mariani, and A. Ruocco, *Measurement Science and Technology* **33**, 025102 (2021).
- [12] A. Apponi, G. Cavoto, M. Iannone, C. Mariani, F. Pandolfi, D. Paoloni, I. Rago, and A. Ruocco, *Journal of Instrumentation* **15**, P11015 (2020).
- [13] M. Gugiatti, M. Biassoni, M. Carminati, O. Cremonesi, C. Fiorini, P. King, P. Lechner, S. Mertens, L. Pagnanini, M. Pavan, *et al.*, *Nuclear Instruments and Methods in Physics Research Section A: Accelerators, Spectrometers, Detectors and Associated Equipment* **979**, 164474 (2020).
- [14] L. Manenti, C. Pepe, I. Sarnoff, T. Ibrayev, P. Oikonomou, A. Knyazev, E. Monticone, H. Garrone, F. Alder, O. Fawwaz, *et al.*, *Physical Review Applied* **22**, 024051 (2024).
- [15] K. Patel, S. Withington, A. Shard, D. Goldie, and C. Thomas, *Journal of Applied Physics* **135**, 224504 (2024).
- [16] M. Loidl, J. Beyer, L. Bockhorn, C. Enss, S. Kempf, K. Kossert, R. Mariam, O. Nähle, M. Paulsen, P. Ranitzsch, *et al.*, *Applied Radiation and Isotopes* **153**, 108830 (2019).
- [17] R. P. Fitzgerald, B. K. Alpert, D. T. Becker, D. E. Bergeron, R. M. Essex, K. Morgan, S. Nour, G. O’Neil, D. R. Schmidt, G. A. Shaw, *et al.*, *Journal of Research of the National Institute of Standards and Technology* **126**, 126048 (2022).
- [18] M. Betti, M. Biasotti, A. Boscá, F. Calle, J. Carabe-Lopez, G. Cavoto, C. Chang, W. Chung, A. Cocco, A. Colijn, *et al.*, *Progress in Particle and Nuclear Physics* **106**, 120 (2019).
- [19] M. Betti, M. Biasotti, A. Boscá, F. Calle, N. Canci, G. Cavoto, C. Chang, A. Cocco, A. Colijn, J. Conrad, *et al.*, *Journal of Cosmology and Astroparticle Physics* **2019**, 047 (2019).
- [20] A. Apponi, M. Betti, M. Borghesi, N. Canci, G. Cavoto, C. Chang, W. Chung, A. Cocco, A. Colijn, N. D’Ambrosio, *et al.*, *Journal of Instrumentation* **17**, P05021 (2022).
- [21] C. Pepe, B. Corcione, F. Pandolfi, H. Garrone, E. Monticone, I. Rago, G. Cavoto, A. Apponi, A. Ruocco, F. Malnati, *et al.*, *Physical Review Applied* **22**, L041007 (2024).
- [22] B. Corcione, *Il Nuovo Cimento C* **48**, 187 (2025), published online 26 August 2025.
- [23] D. Drung, C. Abmann, J. Beyer, A. Kirste, M. Peters, F. Ruede, and T. Schurig, *IEEE Transactions on Applied Superconductivity* **17**, 699 (2007).
- [24] L. Cecchini, C. Pepe, B. Corcione, O. Castellano, D. Paoloni, F. Malnati, G. Cavoto, M. Carminati, C. Fiorini, G. Pettinari, *et al.*, *Nanoscale* **17**, 21260 (2025).
- [25] E. Schifano, G. Cavoto, F. Pandolfi, G. Pettinari, A. Apponi, A. Ruocco, D. Uccelletti, and I. Rago, *Nanomaterials* **13**, 1081 (2023).
- [26] R. P. Yadav, I. Rago, F. Pandolfi, C. Mariani, A. Ruocco, S. Tayyab, A. Apponi, and G. Cavoto, *Nuclear Instruments and Methods in Physics Research Section A: Accelerators, Spectrometers, Detectors and Associated Equipment* **1060**, 169081 (2024).
- [27] F. Sarasini, J. Tirillò, M. Lilli, M. P. Bracciale, P. E. Vullum, F. Berto, G. De Bellis, A. Tamburrano, G. Cavoto, F. Pandolfi, *et al.*, *Composites Part B: Engineering* **243**, 110136 (2022).
- [28] S. Tayyab, A. Apponi, M. G. Betti, E. Blundo, G. Cavoto, R. Frisenda, N. Jiménez-Arévalo, C. Mariani, F. Pandolfi, A. Polimeni, *et al.*, *Nanomaterials* **14**, 77 (2023).
- [29] R. H. Fowler and L. Nordheim, *Proceedings of the royal society of London. Series A, containing papers of a mathematical and physical character* **119**, 173 (1928).
- [30] R. Gomer, *Surface science* **299**, 129 (1994).
- [31] M. J. Oreglia, *Study of the reactions  $\psi' \rightarrow \gamma\gamma\psi$  [Thesis]*, Tech. Rep. (SLAC National Accelerator Laboratory (SLAC), Menlo Park, CA (United States), 1980).